7-1-2017

Toward Reliable Modeling of S-nitrosothiol Chemistry: Structure and Properties of Methyl Thionitrite (CH3SNO), an S-nitrosocysteine Model

Dmitry Khomyakov
Marquette University

Qadir K. Timerghazin
Marquette University, qadir.timerghazin@marquette.edu

Published version. *The Journal of Chemical Physics*, Vol. 147, No. 4 (July 2017). DOI.

Toward reliable modeling of S-nitrosothiol chemistry: Structure and properties of methyl thionitrite (CH_3SNO), an S-nitrosocysteine model

Dmitry G. Khomyakov and Qadir K. Timerghazin[a)]
Department of Chemistry, Marquette University, Milwaukee, Wisconsin 53201-1881, USA

(Received 9 May 2017; accepted 10 July 2017; published online 25 July 2017)

Methyl thionitrite CH_3SNO is an important model of S-nitrosated cysteine aminoacid residue (CysNO), a ubiquitous biological S-nitrosothiol (RSNO) involved in numerous physiological processes. As such, CH_3SNO can provide insights into the intrinsic properties of the —SNO group in CysNO, in particular, its weak and labile S—N bond. Here, we report an *ab initio* computational investigation of the structure and properties of CH_3SNO using a composite Feller-Peterson-Dixon scheme based on the explicitly correlated coupled cluster with single, double, and perturbative triple excitations calculations extrapolated to the complete basis set limit, CCSD(T)-F12/CBS, with a number of additive corrections for the effects of quadruple excitations, core-valence correlation, scalar-relativistic and spin-orbit effects, as well as harmonic zero-point vibrational energy with an anharmonicity correction. These calculations suggest that the S—N bond in CH_3SNO is significantly elongated (1.814 Å) and has low stretching frequency and dissociation energy values, ν_{S-N} = 387 cm^{-1} and D_0 = 32.4 kcal/mol. At the same time, the S—N bond has a sizable rotation barrier, $\triangle E_0^{\neq}$ = 12.7 kcal/mol, so CH_3SNO exists as a cis- or trans-conformer, the latter slightly higher in energy, $\triangle E_0$ = 1.2 kcal/mol. The S—N bond properties are consistent with the antagonistic nature of CH_3SNO, whose resonance representation requires two chemically opposite (antagonistic) resonance structures, $CH_3—S^+=N—O^-$ and $CH_3—S^-/NO^+$, which can be probed using external electric fields and quantified using the natural resonance theory approach (NRT). The calculated S—N bond properties slowly converge with the level of correlation treatment, with the recently developed distinguished cluster with single and double excitations approximation (DCSD-F12) performing significantly better than the coupled cluster with single and double excitations (CCSD-F12), although still inferior to the CCSD(T)-F12 method that includes perturbative triple excitations. Double-hybrid density functional theory (DFT) calculations with mPW2PLYPD/def2-TZVPPD reproduce well the geometry, vibrational frequencies, and the S—N bond rotational barrier in CH_3SNO, while hybrid DFT calculations with PBE0/def2-TZVPPD give a better S—N bond dissociation energy. *Published by AIP Publishing.* [http://dx.doi.org/10.1063/1.4995300]

I. INTRODUCTION

S-Nitrosothiols (RSNOs) are ubiquitous biological derivatives of nitric oxide, a major gasotransmitter.[1–4] Reversible S-nitrosation of the thiol functional group of cysteine (Cys) aminoacid residues in proteins leading to the formation of S-nitrosated cysteine CysNO is an important post-translational modification involved in numerous biological processes across a wide variety of organisms.[5–13] Thousands of proteins have been reported to undergo S-nitrosation *in vivo*,[6,8,10] and while numerous factors point out to enzymatic control of biological RSNO reactions,[9,14,15] the underlying chemistry is still poorly understood.[4]

RSNOs in general are sensitive to light, rapidly decompose in the presence of metal ions, and have low thermal stability with respect to homolytic cleavage of the weak S—N bond with dissociation energy of only ~30 kcal/mol.[16–18] However, the molecular environment can modulate the stability of CysNO in an exceptionally wide range,[19] likely through the influence of proximal charges.[20,21] For instance, the room-temperature *in vitro* half-life ($t_{1/2}$) of CysNO as a free aminoacid is only 0.5 h; however, it increases to 13.6 h for CysNO residue in a protein albumin and to 40 h for CysNO within a tripeptide glutathione, while N-acetylated CysNO has $t_{1/2}$ = 500 h.[19] Understanding the molecular origins of this remarkable variation of properties as well as the enzymatic mechanisms underlying the biological reactions involving CysNO requires reliable information on the intrinsic properties of the —SNO group in CysNO, in particular the strength of its S—N bond. For instance, reliable data on the S—N bond dissociation energy in CysNO are essential for thermochemical analysis of the biological reactions of nitric oxide and its derivatives.[22] In this context, accurate electronic structure calculations of the relevant CysNO models are certainly of significant value.

Unfortunately, RSNOs do not lend themselves to reliable computational modeling of their properties—in

a)Electronic mail: qadir.timerghazin@marquette.edu

particular, the S—N bond dissociation energy, whose early computational predictions ranged from 15 to 35 kcal/mol depending on the method.[23,24] Later systematic high-level *ab initio* investigations focused on thionitrous acid HSNO,[25–30] the smallest RSNO model molecule that, due to its small size, could be feasibly investigated with the state-of-the-art electronic structure methods. Although HSNO has been recently proposed to be an important biological RSNO in its own right,[31–33] accurate high-level computational—and also recently reported[30] experimental—data on HSNO may have only limited utility for understanding the chemistry of the most biologically abundant cysteine-based RSNOs since the nature of substituent R may significantly affect the properties of the —SNO group.[19,34]

The smallest aliphatic RSNO, methyl thionitrite CH_3SNO, is a far better model of S-nitrosated cysteine sidechain, a primary aliphatic RSNO. As the prior computational investigations of HSNO have demonstrated,[25,26,28] the computed —SNO group properties show excruciatingly slow convergence with respect to the level of the electron correlation treatment and the one-electron basis set size, necessitating using coupled cluster methods with excitations up to quadruple level and one-electron basis sets up to quintuple- (5Z) and sextuple-zeta (6Z) quality. This made accurate *ab initio* calculations of even marginally larger CH_3SNO molecule extremely challenging computationally.

Fortunately, recently developed explicitly correlated (F12) coupled cluster methods now allow to significantly alleviate the one-electron basis set convergence problems.[35,36] The F12 methods that explicitly include inter-electron distance through an exponential correlation factor $F_{12} = e^{-\gamma r_{12}}$ demonstrate much faster convergence to the complete basis set limit (CBS), so sextuple-zeta (6Z) quality results can be achieved with quadruple-zeta (QZ) basis set and quintuple-zeta (5Z) quality—with triple-zeta (TZ) basis set, the "two-zeta gain rule."[37] Promising preliminary data on the explicitly correlated coupled cluster calculations of HSNO[27,38] suggests that this rule also holds in the challenging case of the —SNO group.

Therefore, in this work, we report accurate *ab initio* investigation of CH_3SNO molecule with the Feller-Peterson-Dixon (FPD) approach,[39–41] based on the CBS-extrapolated explicitly correlated coupled cluster with single, double, and perturbative triple excitations, CCSD(T)-F12, calculations with a number of additive corrections for the effects of quadruple excitations, core-valence correlation, scalar-relativistic and spin-orbit effects, as well as harmonic zero-point vibrational energy (ZPE) with an anharmonicity correction. In particular, we focus on the S—N bond properties—its length, vibrational frequency, dissociation energy, and the rotational barrier; we also examine the convergence of these properties with the level of the coupled-cluster electron correlation treatment, including recently developed distinguished cluster approach, and discuss the unusual antagonistic nature of the S—N bond probed through external electric field effect calculations. We also report a limited assessment of the performance of several commonly used density functional theory (DFT) methods against the high-level FPD data.

II. COMPUTATIONAL DETAILS

Ab initio electronic structure calculations were performed using Molpro 2015.1[42] program package and MRCC code interfaced with the CFOUR program[43,44] that was used for CCSDT(Q) calculations. Full geometry optimizations of *cis*- and *trans*-CH_3SNO and CH_3SNO cis-trans isomerization transition state ($TS_{c\text{-}t}$) were performed using frozen-core fixed amplitude explicitly correlated (F12) coupled-cluster with single, double, and perturbative connected triple excitations, CCSD(T)-F12,[35,36] with the F12-optimized cc-pV*n*Z-F12 (n = D, T, and Q; further referred to as VDZ-F12, VTZ-F12, and VQZ-F12, respectively) basis sets,[45] and the nature of all stationary points was confirmed by vibrational frequency calculations using the Hessian matrix evaluated numerically. In addition, performance of coupled-cluster with single and double excitations, CCSD-F12,[35,36] as well as conventional and explicitly correlated distinguishable cluster with single and double excitations. DCSD and DCSD-F12[46–48] has been investigated.

The complete basis set (CBS) extrapolations were performed based on the CCSD(T)-F12/VTZ-F12 (n = 3) and CCSD(T)-F12/VQZ-F12 (n = 4) results using a two-point formula[49]

$$E(n) = E_{CBS_{(T-Q)}} + \frac{B}{n^3}, \tag{1}$$

which has been applied directly to estimate the geometric parameters at the CBS limit. The corrections for the coupled cluster quadruple excitations, △(Q), were evaluated by initial geometry optimization at the CCSD(T)/cc-pV(D+d)Z level followed by the S—N bond relaxation with the CCSDT(Q)/cc-pV(D+d)Z level. Core-valence corrections (△CV) to the geometric parameters were estimated from all-electron (excluding the 1s-electrons of S atom) and frozen-core CCSD(T)-F12 geometry optimizations with weighted CV basis set cc-pCVTZ-F12.[50] Scalar-relativistic corrections △SR were evaluated in a similar manner at the CCSD(T)/cc-pVQZ-DK level using the Douglas-Kroll-Hess method,[51,52] as implemented in Molpro.

Calculations of the energetic parameters, D(S—N), $\triangle E$(cis-trans), and $\triangle E^{\neq}$(cis-trans), were based on the CCSD(T)-F12/CBS electronic energies and harmonic zero-point vibrational energies (ZPE_{harm}) calculated with two-point $CBS_{(T\text{-}Q)}$ extrapolation formula (1), using the CCSD(T)-F12a/VTZ-F12 and CCSD(T)-F12a/VQZ-F12 data. We compared the $CBS_{(T\text{-}Q)}$ values of D_e(S—N), obtained with the two-point formula (1) and a Schwenke-type extrapolation scheme (2),[53]

$$E_{CBS} = (E_{large} - E_{small})F + E_{small}, \tag{2}$$

where E_{large} and E_{small} correspond to the electronic energies, obtained with VTZ-F12 and VQZ-F12 basis sets, correspondingly. Hill *et al.*[54] proposed the F value in (2) as 1.363 388 for the CCSD-F12 with the VTZ-F12/VQZ-F12 basis sets, and 1.769 474 for the perturbative (T) contribution, intending to alleviate slower convergence of the (T) component on the one-electron basis set size. In this work, both schemes produced nearly identical results (Table S1 in the supplementary material).

The △(Q) corrections for NO˙ and CH_3S˙ radicals were obtained from single-point calculations with the cc-pV(D+d) basis set, whereas the S—N bond length in CH_3SNO was optimized at the CCSDT(Q) level. △CV and △SR corrections were calculated with full geometry optimization of *cis*-CH_3SNO and the radical fragments. Spin-orbit coupling correction for the CH_3S˙ radical (△SO) was calculated with the Breit-Pauli operator,[55] with the multireference configuration interaction (MRCI) method[56,57] and aug-cc-pV(Q+d)Z basis set,[58,59] as implemented in Molpro.

All density functional theory (DFT) calculations were performed with Gaussian 09 and Gaussian 16[60] electronic structure packages, with "UltraFine" settings for the integration grid (99 radial shells, 590 angular points per shell), with a number of hybrid functionals including B3LYP,[61–63] PBE0,[64–66] PBE0 with empirical dispersion correction,[67] PBE0-D3, PBE0 with increased exact exchange contribution, PBE0-1/3,[68] ωB97XD,[69] as well as double-hybrid PBE0DH,[70] PBE0QIDH,[71] B2PLYP,[72] mPW2PLYP[73] functionals and their dispersion-corrected versions B2PLYPD and mPW2PLYPD.[73]

DFT calculations used def2-SV(P)+d [with a tight d-type basis function for sulfur from the aug-cc-pV(D+d)Z basis set[59]] and def2-TZVPPD basis sets by Weigend and Ahlrichs.[74,75] Natural Resonance Theory (NRT)[76,77] calculations were performed with the NBO 5.9 code,[78] using PBE0/def2-TZVPPD density matrices. The contributions of the three resonance structures (***S***, ***D*** and ***I***, see below) were determined from optimized multi-reference weights, as implemented in the multi-reference NRT[76] procedure.

The anharmonic contributions to vibrational frequencies and ZPE used in the FPD scheme were calculated with second-order perturbation theory (PT2) approach,[79] at the mPW2PLYPD/def2-TZVPPD and PBE0-GD3/def2-TZVPPD levels. The solvent effects on the FPD energetic parameters were evaluated from DFT calculations with the def2-TZVPPD basis set and the integral equation formalism polarizable continuum model (IEFPCM),[80] with parameters for water (ε = 78.36) and diethylether (ε = 4.24).

III. STRUCTURE OF CH_3SNO

Accurate *ab initio* calculations of the RSNO properties—in particular, those of the S—N bond—are challenging due to slow convergence with respect to both one-electron basis set size and the level of electron correlation treatment.[25,28] For instance, in our earlier study of HSNO, improving the basis set from double- to quintuple-zeta lead to >0.05 Å shortening in the S—N bond length *r*(S—N) at the CCSD level (1.856 Å and 1.800 Å, respectively), while improving the correlation treatment from CCSD to CCSD(T) lead to >0.04 Å lengthening (1.800 Å and 1.841 Å with quintuple-zeta basis set).

In this work, we applied explicitly correlated (F12) coupled cluster methods instead of conventional coupled cluster approaches used earlier for HSNO modeling.[25,28] This methodological improvement largely solved the slow convergence with respect to the one-electron basis set size. Indeed, the *r*(S—N) values obtained with a double zeta VDZ-F12 basis set overestimate the corresponding CBS-extrapolated values (obtained with the same coupled-cluster method) by just ~0.003 Å. Similar to HSNO,[25] the coupled-cluster methods with a different level of electron correlation treatment demonstrate smooth and generally parallel convergence with respect to the one-electron basis set size [Fig. 1(a), Table I, Tables S2-S3 of the supplementary material].

At the same time, the calculated *r*(S—N) values demonstrate slow convergence with the excitation level included in the coupled cluster calculations; the better the correlation treatment, the longer the S—N bond [Fig. 1(a)]. At the CCSD-F12/CBS level, *r*(S—N) = 1.764 Å, while at the CCSD(T)-F12/CBS level, *r*(S—N) = 1.794 Å, a 0.03 Å increase; the correction to include the effect of perturbative quadruple excitations △(Q), estimated from limited optimization of the S—N bond in CH_3SNO, further lengthens the S—N bond by

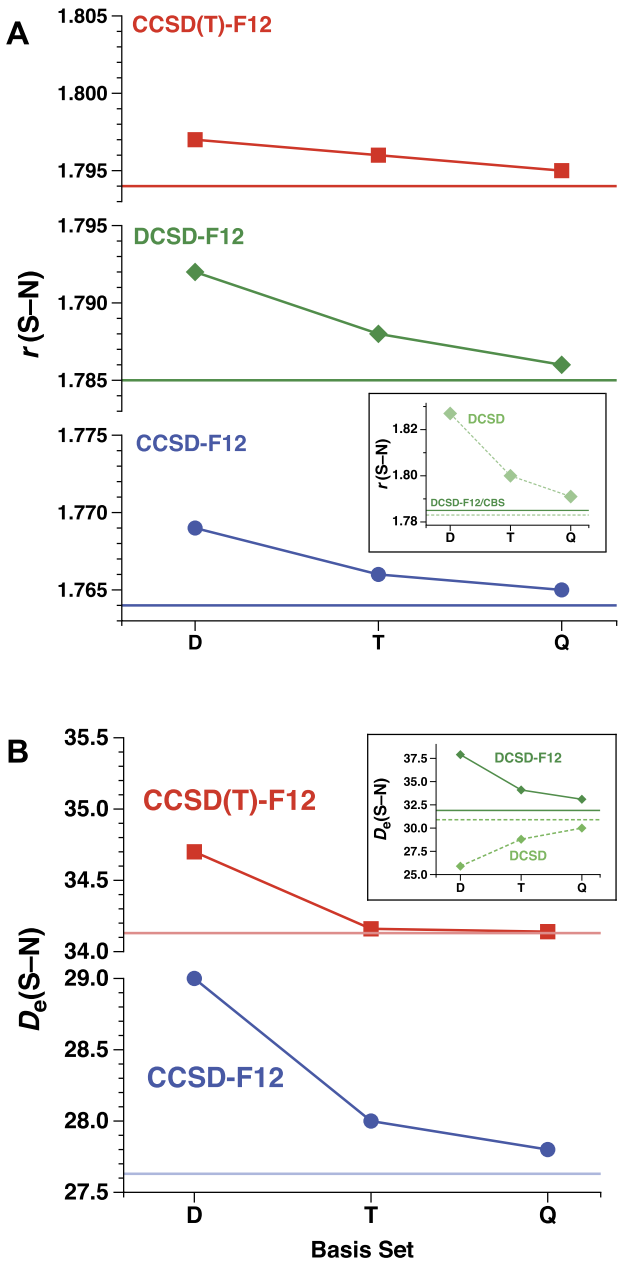

FIG. 1. Basis set convergence (D, T, Q in cc-pVnZ-F12) of the S—N bond lengths (a) and D_e(S—N) in*cis*-MeSNO (b). The horizontal lines show the respective CBS(T-Q) limits.

TABLE I. FPD geometric parameters of CH_3SNO conformers.

Parameter	CCSD(T)-F12/CBS$_{(T-Q)}$	△(Q)	△CV	△SR	Final FPD value
		cis-CH_3SNO			
r(S—N) (Å)	1.794	0.023	−0.007	0.005	1.814
r(N—O) (Å)	1.191	...	−0.002	−0.001	1.189
r(C—S) (Å)	1.791	...	−0.004	0.002	1.789
∠SNO (deg)	117.42	...	0.08	−0.06	117.45
∠CSN (deg)	102.33	...	0.10	−0.12	102.31
		trans-CH_3SNO			
r(S—N) (Å)	1.799	0.026	−0.005	0.004	1.824
r(N—O) (Å)	1.188	...	−0.002	−0.001	1.186
r(C—S) (Å)	1.797	...	−0.005	0.002	1.795
∠SNO (deg)	115.62	...	0.001	−0.06	115.56
∠CSN (deg)	94.98	...	0.10	−0.10	94.98
		Cis-trans isomerization TS			
r(S—N) (Å)	1.955	0.026	−0.007	0.006	1.980
r(N—O) (Å)	1.167	...	−0.002	−0.001	1.165
r(C—S) (Å)	1.809	...	−0.004	0.002	1.806
∠SNO (deg)	113.07	...	0.02	−0.03	113.06
∠CSN (deg)	90.85	...	0.10	−0.18	90.77
∠CSNO (deg)	85.39	...	−0.01	0.06	85.44

0.023 Å. This behavior points out to an appreciable multi-reference character of the —SNO group earlier noted in the case of HSNO.[25,28,81] The T_1 and D_1 coupled cluster diagnostic values (Table S4 of the supplementary material) that can be used to assess the multireference character of a molecule[82,83] are similar for CH_3SNO and HSNO molecules: T_1 = 0.025 and D_1 = 0.080 for *cis*-CH_3SNO and T_1 = 0.026 and D_1 = 0.077 for *cis*-HSNO,[28] above the accepted thresholds of 0.02 and 0.05, respectively, which suggests a moderate multi-reference character in both cases. A slightly smaller value of the T_1 diagnostic and smaller effects of the triple (+0.030 Å in *cis*-CH_3SNO vs +0.041 Å in *trans*-HSNO[25]) and quadruple (+0.023 Å in *cis*-CH_3SNO vs +0.033 Å in *trans*-HSNO[28]) excitations may suggest marginally reduced multi-reference character of CH_3SNO compared to HSNO.

We also investigated the performance of recently developed distinguishable cluster with single and double excitations (DCSD) method by Kats *et al.*,[46–48] which at a similar computational cost demonstrated significant improvement over CCSD for multi-reference systems. In the case of CH_3SNO, DCSD-F12 indeed provides better description of the S—N bond length than CCSD-F12, 1.785 Å vs. 1.764 Å, a +0.021 Å improvement, just below (−0.009 Å) the CCSD(T)-F12 value of 1.794 Å. A conventional DCSD method shows expectedly slower convergence [Fig. 1(a), inset] but appears to converge to roughly the same CBS limit as DCSD-F12.

The CCSD(T)-F12/CBS+△Q geometries were further corrected to include core-valence correlation △CV and scalar-relativistic effects △SR. The former shortens the S—N bond in *cis*-CH_3SNO by 0.007 Å, while the latter elongates it by 0.005 Å (−0.005 Å and 0.004 Å in *trans*-CH_3SNO). The final FPD values of r(S—N) in CH_3SNO, 1.814 Å in *cis*-CH_3SNO and 1.824 Å in *trans*-CH_3SNO, are noticeably shorter than our recent FPD values for HSNO, 1.842 Å in *cis*-HSNO and 1.858 Å in *trans*-HSNO, as well as recent semi-experimental values by Nava *et al.*,[30] 1.834(2) Å in *cis*-HSNO and 1.852(2)Å in *trans*-HSNO, derived from the experimental ground-state rotational constants corrected for zero-point vibrational motion using CCSD(T)/aug-cc-pV(Q+d)Z calculations.

The N—O bond length in RSNOs is less sensitive to the basis set size, e.g., for HSNO[28] even conventional CCSD(T) calculations with a triple-zeta basis set give a reasonable approximation to the CBS limit (1.183 Å and 1.180 Å, respectively).[28] Not surprisingly, r(N—O) obtained with explicitly correlated CCSD(T)-F12 converge almost instantly to the CBS limit. In *cis*-CH_3SNO, even the smallest basis set VDZ-F12 provides an acceptable N—O bond value of 1.193 Å, just within 0.002 of the corresponding CBS limit of 1.191 Å. With respect to the correlation treatment, the N—O bond elongates by 0.008 Å when going from CCSD-F12 to CCSD(T)-F12 (1.183 Å and 1.191 Å at the CBS limit, respectively), which is significantly smaller than the corresponding S—N bond elongation, 0.03 Å. At the DCSD-F12/CBS level, the N—O bond length (1.190 Å) is almost identical to the CCSD(T)-F12 value. Other CH_3SNO geometry parameters demonstrate even less sensitivity to the level of theory. The C—S bond length calculated at the CCSD(T)-F12/VDZ-F12 level is the same as the extrapolated CCSD(T)-F12/CBS value (1.791 Å). Both △CV and △SR corrections to r(N—O) do not exceed 0.002 Å in magnitude and 0.005 Å in the case of the C—S bond. Figure 2 summarizes the final recommended FPD geometries of the *cis*- and *trans*-CH_3SNO molecules obtained here.

IV. S—N BOND DISSOCIATION ENERGY IN CH_3SNO

The weakness of the S—N bond which makes it prone to homolytic dissociation (many primary and secondary RSNOs have half-lives from seconds to minutes[84]) is one of the defining features of the RSNO chemistry. This makes the S—N bond homolytic dissociation energy in RSNOs one of the most important parameters, which, at the same time, is also challenging to accurately predict computationally due to slow

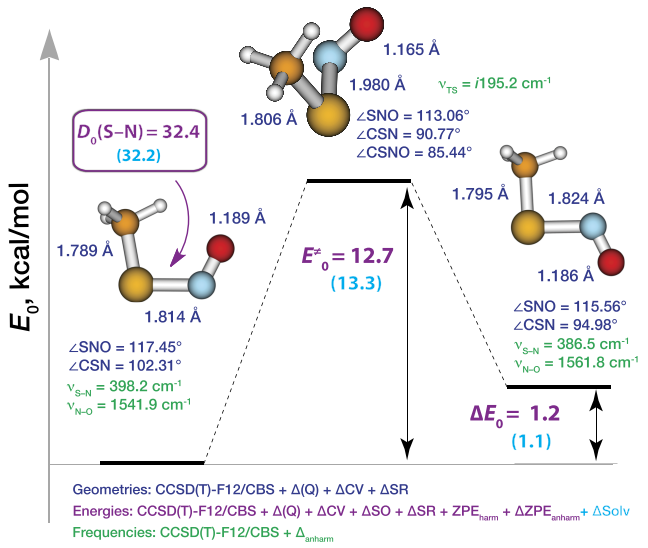

FIG. 2. Recommended *ab initio* geometric and energetic parameters of *cis*-CH_3SNO (left), $TS_{c\text{-}t}$ (middle), and *trans*-CH_3SNO (right).

convergence with respect to the basis set size and the degree of correlation treatment. In our earlier conventional coupled cluster studies of HSNO,[25,28] double- to quintuple-zeta basis set improvement increased D_e(S—N) by >5 kcal/mol (22.6 and 27.8 kcal/mol at the CCSD level). Improving the electron correlation treatment to perturbatively include the effect of triple excitations further increased D_e(S—N) by >5.5 kcal/mol (31.4 kcal/mol with quintuple-zeta basis set), while inclusion of perturbative quadruple excitations (evaluated with a double-zeta basis set) increased it by another ~1.3 kcal/mol.[25,28]

Explicitly correlated coupled cluster methods expectedly improve the D_e(S—N) convergence with respect to the basis set size. For *cis*-CH_3SNO, the D_e(S—N) values obtained at the CCSD-F12 level with VDZ-F12 and VQZ-F12 differ only by 1.2 kcal/mol [29.0 vs. 27.7 kcal/mol, Fig. 1(b) and Table S5 of the supplementary material]; the convergence is even faster at the CCSD(T)-F12 level, for which the VDZ-F12 and VQZ-F12 results differ by 0.6 kcal/mol (34.7 vs. 34.1 kcal/mol). Interestingly, the D_e(S—N) values calculated with F12 converge to the CBS limit from above, i.e., smaller basis set calculations overestimate D_e(S—N). On the other hand, D_e(S—N) values for HSNO obtained with conventional coupled cluster calculations[25,28] converged from below, with smaller basis sets underestimating D_e(S—N).

The level of correlation treatment has a dramatic effect on the D_e(S—N) value, with CCSD(T)-F12 giving ~6.5 kcal/mol stronger S—N bond than CCSD-F12 (34.1 vs. 27.7 kcal/mol at the CBS limit, Table S5 of the supplementary material); including the effect of quadruple excitations △(Q) further increases D_e(S—N) by 1.33 kcal/mol (Table II and Table S6 of the supplementary material). At the extrapolated CBS limit, DCSD-F12 performs better than CCSD-F12, giving 4.2 kcal/mol higher D_e(S—N) value (31.9 vs. 27.7 kcal/mol), but still 2.2 kcal/mol below the CCSD(T)-F12/CBS value (34.1 kcal/mol). Similar to explicitly correlated CCSD-F12 and CCSD(T)-F12, D_e(S—N) calculated with DCSD-F12 converge to the CBS limit from above. However, the explicitly correlated DCSD-F12 demonstrates much worse convergence

TABLE II. FPD energy properties of CH_3SNO conformers, kcal/mol.

FPD component	D(S—N)	$\Delta E_{\text{cis-trans}}$	$\Delta E^{\neq}_{\text{cis-trans}}$
CCSD(T)-F12/CBS$_{(T\text{-}Q)}$	34.1	1.15	12.61
△(Q)	1.33	−0.06	0.56
△CV	−0.02	0.01	0.10
△SO	−0.18	...	...
△SR	−0.41	0.00	−0.07
ZPE$_{harm}$	−2.79	0.04	−0.55
△ZPE$_{anharm}$	0.38	0.01	...
Final FPD value	32.4	1.15	12.65

of D_e(S—N) with the basis set size. Surprisingly, the conventional version of DCSD demonstrates slightly better convergence: increasing the basis set size from VDZ-F12 to VQZ-F12 decreases D_e(S—N) by 4.8 kcal/mol in the case of DCSD-F12, and it increases D_e(S—N) by 4.1 kcal/mol in the case of conventional DCSD. As in the case of other coupled cluster methods, the D_e(S—N) values approach to the CBS limit from below with the conventional DCSD and from above with DCSD-F12. Both methods appear to converge roughly to the same CBS value, although due to the slow basis set convergence the CBS$_{(T\text{-}Q)}$ extrapolations are much less reliable than in the case of CCSD-F12 and CCSD(T)-F12 methods.

The core-valence electron correlation correction △CV to the D_e(S—N) value is minor (−0.02 kcal/mol, Table II), while the scalar-relativistic correction reduces D_e(S—N) by 0.41 kcal/mol. Due to the relatively high spin-orbit coupling constant of sulfur (1.13 kcal/mol)[85] and the open-shell character of $CH_3S^{\bullet}$ radical, the D_e(S—N) value needs to be corrected for extra stabilization of the $CH_3S^{\bullet}$ radical due to spin-orbit coupling, △SO. However, the △SO correction for D_e(S—N) is more than two-fold smaller for CH_3SNO vs. the △SO correction reported earlier for HSNO,[25] 0.18 kcal/mol vs. 0.48 kcal/mol. This is because Jahn-Teller geometry distortion removes the degeneracy of the two lowest electronic states of $CH_3S^{\bullet}$, so the energy gap between non-degenerate $^2A'$ and $^2A''$ states in C_s-symmetry $CH_3S^{\bullet}$ is 1.54 kcal/mol [at the MRCI/aug-cc-pV(Q+d)Z level, Fig. S1 in the supplementary material]. On the other hand, HS· radical has two degenerate $^2\Pi$ states which leads to stronger spin-orbit coupling.

The zero-point vibrational energy (ZPE) effect on the the S—N bond dissociation energy in CH_3SNO is mostly determined by the S—N stretching vibration, so the ZPE$_{harm}$ correction obtained from harmonic frequency calculations at the CCSD(T)-F12/VQZ-F12 level is similar to the HSNO case,[28] −2.79 kcal/mol and −2.77 kcal/mol, respectively. The ZPE$_{harm}$ value has been further corrected to anharmonicity, △ZPE$_{anharm}$, evaluated with the second-order perturbative approach[79] using the double-hybrid mPW2PLYPD/def2-TZVPPD DFT method. With this correction, our final FPD value D_0(S—N) for CH_3SNO in the gas phase is 32.4 kcal/mol.

For a better comparison of the S—N bond strength in CH_3SNO vs. HSNO, we updated the FPD value of D_0(S—N) reported earlier for HSNO (29.4 kcal/mol),[28] to include the anharmonicity correction △ZPE$_{anharm}$ recently evaluated[38] with vibrational configuration interaction (VCI) method[86,87] at the CCSD(T)-F12/VDZ-F12 level,

$\triangle ZPE_{anharm}$ = −0.29 kcal/mol, which compares very well with the second-order perturbative estimate at the mPW2PLYPD/def2-TZVPPD level, −0.28 kcal/mol. The updated FPD estimate of D_0(S—N) for HSNO is then 29.7 kcal/mol.

Thus, the gas-phase FPD values suggest that the S—N bond in CH_3SNO is at least 2.7 kcal/mol more stable than that in HSNO. We note that the correction for quadruple excitations △(Q) was evaluated in this work using partially optimized CH_3SNO geometry (only the S—N bond was relaxed due to the computational limitations), which tends to underestimate △(Q) by 0.02-0.03 kcal/mol.[28] Therefore, the D_0(S—N) = 32.4 kcal/mol value is best considered as a lower bound for the actual value that is slightly larger (by a few tenths kcal/mol).

Finally, to make the data obtained in this work more relevant for assessing the stability of the cysteine-based biological RSNOs in the aqueous environment, we evaluated the solvation effects △Solv on D_0(S—N) using DFT calculations with a polarizable continuum model (PCM). These calculations (Table S7 of the supplementary material) suggest a small decrease of D_0(S—N) in water (−0.17 kcal/mol) and diethylether which is often used to mimic protein environment (−0.15 kcal/mol); this suggests D_0(S—N) = 32.2 kcal/mol for CH_3SNO in solution.

V. CONFORMATIONAL BEHAVIOR OF CH_3SNO

The predisposition of RSNOs to adapt planar conformations of the —SNO fragment due to the hindered rotation around the S—N bond has been noted in numerous early experimental studies.[88–90] Cis-trans isomerism of CH_3SNO was reported as early as in 1961 based on the IR spectroscopic data,[91] followed by the observation of cis-trans conformational change in CH_3SNO in low-temperature proton NMR experiments,[92] and IR spectroscopy in argon matrix.[93] Recent gas-phase IR studies demonstrated 3:1 cis/trans ratio for another primary RSNO, CH_3CH_2SNO,[94] whereas this ratio is inverted (1:4) for tertiary $(CH_3)_3CSNO$.[95]

The FPD data on the relative stability of *cis*-CH_3SNO and *trans*-CH_3SNO (Table II) suggest that the *cis*-conformer is slightly more stable, $\triangle E_0$(cis-trans) = 1.15 kcal/mol, which is typical for primary RSNOs. On the other hand, HSNO prefers trans-conformation by 0.9 kcal/mol.[28] The $\triangle E_0$(cis-trans) value is generally not sensitive to the level of theory (Table II and Table S8 of the supplementary material) and has low sensitivity to the solvent effects (*trans*-CH_3SNO stability increases by ∼0.02 kcal/mol in water and diethylether, Table S7 of the supplementary material).

We were also able to optimize and characterize the transition structure $TS_{c\text{-}t}$ of CH_3SNO cis-trans interconversion with the FPD approach (Table I and Table S9 of the supplementary material). The S—N bond in the $TS_{c\text{-}t}$ level is noticeably elongated compared to *cis*-CH_3SNO, by 0.13-0.16 Å, depending on the level of theory; otherwise, the evolution of r(S—N) and other $TS_{c\text{-}t}$ geometric parameters with increasing one-electron basis set and the level of electron correlation treatment as well as the magnitudes of the △(Q), △CV, and △SR corrections are comparable to the S—N bond in the equilibrium CH_3SNO structures. The final FPD r(S—N) value for $TS_{c\text{-}t}$, 1.980 Å, is 0.166 Å longer than in *cis*-CH_3SNO. The $TS_{c\text{-}t}$ structure is slightly non-perpendicular, with the CSNO dihedral angle 85.4°.

The activation barrier of *cis-trans* CH_3SNO interconversion $\triangle E_e^{\neq}$ is relatively insensitive to the basis set size, and slightly increases with the level of electron correlation treatment (Table S10 of the supplementary material). CCSD-F12/CBS predicts $\triangle E_e^{\neq}$ of 11.8 kcal/mol, DCSD-F12/CBS gives 12.0 kcal/mol, CCSD(T)-F12/CBS gives 12.6 kcal/mol, and addition of the quadruple excitations correction △(Q) raises $\triangle E_e^{\neq}$ to 13.2 kcal/mol; parallel to this progression, the S—N bond lengthens from 1.894 Å to 1.978 Å.

Inclusion of the △CV and △SR corrections (+0.1 and −0.07 kcal/mol, respectively), as well as a ZPE_{harm} correction (−0.55 kcal/mol) gives the final FPD value for the cis-trans interconversion barrier, $\triangle E_0^{\neq}$ = 12.65 kcal/mol.

Previous FPD investigation[28] of HSNO yielded noticeably a lower value of the rotational barrier along the S—N bond, $\triangle E_0^{\neq}$ = 9.52 kcal/mol. In the case of HSNO, the S—N bond elongation in the corresponding TS is larger than in the case of CH_3SNO (0.175 Å vs. 0.166 Å), and the TS structure itself has a more upright geometry with the HSNO dihedral angle 88.0° vs. CSNO dihedral 85.4°.

Finally, the evaluation of the solvation effects on the CH_3SNO cis-trans interconversion barrier using the PCM DFT approach (Table S7 of the supplementary material) suggests that polar and non-polar solvents pull the activation barrier in different directions: aqueous environment on average increases the barrier by 0.57 kcal/mol to $\triangle E_0^{\neq}$ = 13.22 kcal/mol, whereas a less polar solvent (diethylether) decreases the barrier by 0.12 kcal/mol to $\triangle E_0^{\neq}$ = 12.63 kcal/mol.

VI. CH_3SNO VIBRATIONAL FREQUENCIES

CH_3SNO was first characterized in the gas phase by IR spectroscopy in 1961 by Philippe.[91] At that time, only a few fundamental frequencies in the IR spectrum were assigned, and the S—N and N—O bond stretches were assigned to 655 cm^{-1} and 1534 cm^{-1}, respectively. Later, Christensen *et al.*[92] tentatively assigned the S—N—O bending band at 375 cm^{-1}, S—N stretching at 734 cm^{-1}, and N—O stretching at 1530 cm^{-1}. In 1984, Müller and Huber[93] reported the spectra of both *cis*-CH_3SNO and *trans*-CH_3SNO in argon matrix at 12 K, with the N—O band at 1527 cm^{-1} for *cis*-CH_3SNO and 1548 cm^{-1} for *trans*-CH_3SNO (21 cm^{-1} difference), and the S—N band at 376 cm^{-1} for *cis*-CH_3SNO and 371 cm^{-1} for *trans*-CH_3SNO. Recently, Cánneva *et al.*[94] reported gas-phase N—O stretching frequencies of 1537 cm^{-1} and 1559 cm^{-1} (22 cm^{-1} difference) for cis- and trans-conformers of related species, CH_3CH_2SNO.

Here, we calculated harmonic vibrational frequencies for CH_3SNO using CCSD(T)-F12/V*n*Z-F12 (n = D, T, Q) with subsequent two-point $CBS_{(T\text{-}Q)}$ extrapolation (Table III and Tables S11-S12 of the supplementary material). The CCSD(T)-F12 harmonic vibrational frequencies of CH_3SNO demonstrate fast convergence with the basis set size, with the VDZ-F12 values already near the CBS limit (the S—N bond stretch frequency in *cis*-CH_3SNO is 400.6 cm^{-1} vs. 399.7 cm^{-1}, N—O bond stretch frequency is 1571.5 vs. 1575.1 cm^{-1}); and the ZPE_{harm} values obtained with the

TABLE III. *cis*-CH_3SNO and *trans*-CH_3SNO FPD vibrational frequencies.

	CCSD(T)-F12/$CBS_{(T-Q)}$	△Anh.	Final FPD value (vs. Ref. 93)	CCSD(T)-F12/$CBS_{(T-Q)}$	△Anh.	Final FPD value (vs. Ref. 93)
Mode	*cis*-CH_3SNO			*trans*-CH_3SNO		
1 A″	84.6	−39.6	45.1	119.5	−17.3	102.2
2 A′	280.1	−10.0	270.1(268.0)	227.5	−6.9	220.6(234.5)
3 A″	291.0	−4.8	286.2	235.6	−11.1	224.5
4 A′ (S—N)	399.7	−1.5	398.2(376.0)	394.2	−7.6	386.5(371.0)
5 A′	662.4	−9.5	652.9(649.0)	669.6	−9.5	660.1(651.0)
6 A′	754.3	−16.4	737.9(731.5)	751.8	−14.7	737.1(736.5)
7 A′	962.5	−22.8	939.7	1011.0	−16.3	994.7
8 A″	970.8	−12.8	958.0(940.0)	953.5	−17.8	935.7(971.5)
9 A′	1334.3	−35.2	1299.1(1298.0)	1352.6	−32.9	1319.7(1314.0)
10 A″	1477.2	−41.3	1436.0(1428.5)	1468.3	−41.7	1426.6(1441.0)
11 A′	1480.8	−44.7	1436.1(1455.0)	1494.5	−42.4	1452.1(1456.0)
12 A′ (N—O)	1575.1	−33.2	1541.9(1527.0)	1593.5	−31.8	1561.8(1548.0)
13 A′	3028.4	−96.8	2931.6(2910.0)	3046.2	−98.2	2948.0(2909.0)
14 A′	3127.3	−137.3	2990.0(2928.0)	3142.3	−138.9	3003.4(2928.5)
15 A″	3157.2	−145.3	3011.9(2932.0)	3150.6	−144.2	3006.4(2931.5)
ZPE, kcal/mol	28.0	−0.4	27.1	28.0	−0.4	27.1

VDZ-F12 basis set are within 0.1 kcal/mol of the CBS limit. We further corrected the harmonic values by adding a correction for anharmonicity determined with the second-order perturbative approach[79] using the double-hybrid mPW2PLYPD/def2-TZVPPD DFT method (Table S13 of the supplementary material). The resulting vibrational frequencies and ZPE_{anharm} values for *cis*-CH_3SNO are listed in Table III along with available experimental data.[93]

Both experimental and FPD frequencies of the S—N bond stretching in CH_3SNO are below 400 cm^{-1} (398.2/376.0 cm^{-1} calculated/experimental for *cis*-conformer , and 386.5/371.0 cm^{-1} for trans-conformer). The calculated N—O stretching frequencies, 1542 cm^{-1} for *cis*-CH_3SNO and 1562 cm^{-1} for *trans*-CH_3SNO, are also in reasonable agreement with the earlier experimental data on CH_3SNO,[93] 1527 cm^{-1} and 1548 cm^{-1}, and in even better agreement with the recent experimental data on CH_3CH_2SNO, 1537 cm^{-1} and 1559 cm^{-1}; the calculated difference in the N—O stretching frequencies for *cis*- and *trans*-CH_3SNO, 20 cm^{-1}, closely matches with the experimental values for CH_3SNO (21 cm^{-1}) and CH_3CH_2SNO (22 cm^{-1}).[94]

Although the S—N bond CH_3SNO is relatively non-rigid, it is quite harmonic: the second-order perturbative anharmonic corrections evaluated at the mPW2PLYPD/def2-TZVPPD level (Table IV) for the S—N stretching vibration are −1.5 cm^{-1} for *cis*-CH_3SNO and −7.6 cm^{-1} for *trans*-CH_3SNO, while the anharmonic corrections for the N—O stretch are somewhat larger, −33.2 cm^{-1} and −31.8 cm^{-1} for *cis*- and *trans*-CH_3SNO, respectively; anharmonic correction lowers the ZPE_{harm} of both CH_3SNO conformers by 0.9 kcal/mol.

VII. PERFORMANCE OF DFT METHODS

We used the high-level *ab initio* data for CH_3SNO generated here to evaluate the performance of common DFT methods with respect to the —SNO group properties. The DFT method performance was tested with two basis sets: a large triple-zeta basis set with two sets of polarization functions def2-TZVPPD[74,75] and a smaller double-zeta def2-SV(P)+d basis set.[74] Since routine DFT calculations typically do not include relativistic effects, we used a modified set of FPD reference data with omitted △SR and △SO corrections; the results

TABLE IV. Performance of the DFT methods (with def2-TZVPPD basis set) vs. truncated FPD scheme for *cis*-CH_3SNO.

Method	*r*(S—N) (Å)	*r*(N—O) (Å)	*r*(C—S) (Å)	∠SNO (deg)	D_0(S—N) (kcal/mol)
CCSD(T)-F12/$CBS_{(T-Q)}$+△(Q)+△CV+ZPE_{harm}	1.810	1.189	1.787	117.51	32.67
B3LYP	1.816	1.182	1.800	117.83	28.92
PBE0	1.779	1.179	1.782	117.91	31.83
PBE0-D3	1.779	1.179	1.783	117.98	32.54
PBE0-1/3	1.760	1.176	1.778	118.14	28.86
PBE0DH	1.757	1.179	1.777	118.07	28.80
PBE0QIDH	1.754	1.184	1.776	118.01	28.75
ωB97XD	1.767	1.181	1.789	118.12	28.94
B2PLYP	1.811	1.190	1.794	117.61	29.21
B2PLYPD	1.812	1.190	1.796	117.72	29.92
mPW2PLYP	1.794	1.188	1.792	117.79	28.32
mPW2PLYPD	1.795	1.188	1.794	117.87	28.83

of the DFT calculations along with the modified FPD reference data are listed in Tables IV and V and Tables S14-S21 of the supplementary material.

Global hybrid Perdew, Burke, and Ernzerhof functional PBE0[64–66] underestimates the S—N bond length in CH_3SNO and in the TS_{c-t} structure by 0.01-0.05 Å and the addition of an empirical dispersion term D3[67] expectedly does not affect the geometry. The PBE0 version with the fraction of exact exchange increased from 1/4 to 1/3, PBE0-1/3, as recently proposed by Guido *et al.*[68] and the range-separated ωB97XD functional with empirical dispersion[69] tend to give even shorter bond lengths. While these functionals also underestimate all other bond lengths, a widely used global hybrid B3LYP functional[61,63] seems to provide an inconsistent description of the —SNO group: it overestimates the S—N bond lengths (by 0.01-0.04 Å) while underestimating the N—O bond lengths (by ~0.01 Å). Double-hybrid B2PLYP (and its dispersion-corrected variant, B2PLYPD)[72,96] method with the def2-TZVPPD basis set gives equilibrium r(S—N) within 0.001 Å of the reference (1.811 Å B2PLYP and 1.810 Å FPD), while the mPW2PLYP/mPW2PLYPD double hybrid approach[73] underestimates equilibrium r(S—N) by 0.015 Å. On the other hand, mPW2PLYP/mPW2PLYPD overestimates the reference r(S—N) = 1.949 Å in the TS_{c-t} structure by 0.01 Å, while B2PLYP/B2PLYPD overestimates it by ~0.04 Å. Surprisingly, recently proposed double-hybrid functionals PBE0DH[70] and PBE0QIDH[71] based on PBE0 hybrid functional do not improve upon the parent functional: both underestimate the S—N bond lengths by >0.04 Å vs 0.01-0.03 in the case of PBE0.

PBE0 gives the best D_0(S—N) value (Table IV), 31.8 kcal/mol with the def2-TZVPPD basis set vs. 32.7 kcal/mol reference, the addition of empirical dispersion in PBE0-D3 (artificially) improves the result even further, 32.5 kcal/mol, while other hybrid and double-hybrid functionals underestimate D_0(S—N) by 3-4 kcal/mol. DFT methods overestimate the rotational barrier for the S—N bond in CH_3SNO by 0.6-2 kcal/mol relative to the reference value $\triangle E_0^{\neq}$ = 12.7 kcal/mol (Table V), with the smallest errors observed for the range-separated ωB97XD hybrid functional (0.6 kcal/mol with the def2-TZVPPD basis set).

The harmonic vibrational frequencies of CH_3SNO are on average better reproduced with the double-hybrid DFT methods (Tables S18-S21 of the supplementary material), e.g., mPW2PLYPD/def2-TZVPPD gives the best S—N (388.4 cm^{-1} vs. 399.7 cm^{-1} reference) and N—O (1578 cm^{-1} vs. 1571 cm^{-1} reference) stretching frequencies. Using smaller def2-SV(P)+d basis set leads to larger errors in computed vibrational frequencies; in particular, the N—O stretching frequency, which often used as a characteristic band in IR spectroscopy studies of RSNOs, is significantly overestimated, e.g., PBE0-D3/def2-SV(P)+d value 1756 cm^{-1} is almost 200 cm^{-1} larger than the reference (1575.1 cm^{-1}).

Overall, DFT methods provide a reasonably accurate description of the —SNO group, especially when a larger basis set used. Consistent with our earlier observations,[20,28,97] PBE0 hybrid functional generally provides a consistent description of RSNO properties; when feasible, PBE0 results can be verified by more computationally demanding double hybrid DFT calculations.

VIII. ANTAGONISTIC NATURE OF CH_3SNO

The paradox of the RSNO S—N bond which is elongated, weak, and has a low stretching frequency, but, at the same time, has a sizable rotation barrier can be viewed as a consequence of the antagonistic nature of the —SNO group. In this context, antagonistic nature implies that two of the three resonance structures required to describe the —SNO group are chemical opposites of each other, or *antagonistic*.[20] These two structures, referred to as ***D*** and ***I*** [Fig. 3(a)], imply opposite bonding patterns (double S=N bond vs. ionic/no bond) and opposite formal charges (e.g., positive versus negative charge on the sulfur atom). This simple model of the RSNO structure has been shown to have a surprising explanatory and predictive power. It elegantly accounts for the extreme malleability of the S—N bond in the presence of charged or neutral Lewis acids and bases,[20,98,99] provides chemically intuitive description of subtle substituent effects in RSNOs,[19,34,100] and explains the ability of RSNOs to engage in two competing reaction modes with the same molecule.[21,97,99,101] The antagonistic paradigm also provides a useful framework for designing novel RSNO reactions[99] as well as RSNOs with desired properties.[19,34,100]

The accurate FPD data on the CH_3SNO structure reported here are consistent with the antagonistic model. Compared to HSNO, the S—N bond is ~0.03 Å shorter (1.814 Å vs 1.842 Å

TABLE V. Performance of the DFT methods (with the def2-TZVPPD basis set) vs. truncated FPD scheme for CH_3SNO TS_{c-t}.

Method	r(S—N) (Å)	r(N—O) (Å)	r(C—S) (Å)	∠SNO (deg)	∠CSNO (deg)	$\triangle E_0^{\neq}$ (kcal/mol)
CCSD(T)-F12/$CBS_{(T-Q)}$+△(Q)+△CV+ZPE_{harm}	1.949	1.166	1.805	113.09	85.42	12.71
B3LYP	1.987	1.155	1.818	113.84	85.39	13.70
PBE0	1.939	1.154	1.800	113.71	85.08	14.62
PBE0-D3	1.939	1.153	1.801	113.72	85.28	14.66
PBE0-1/3	1.912	1.152	1.795	113.67	85.00	14.22
PBE0DH	1.907	1.155	1.794	113.61	85.01	14.28
PBE0QIDH	1.904	1.159	1.794	113.50	84.88	13.93
ωB97XD	1.924	1.157	1.805	113.51	85.70	13.35
B2PLYP	1.984	1.163	1.814	113.63	85.04	13.65
B2PLYPD	1.985	1.162	1.816	113.65	85.34	13.71
mPW2PLYP	1.960	1.161	1.811	113.62	85.06	13.56
mPW2PLYPD	1.961	1.161	1.812	113.62	85.30	13.60

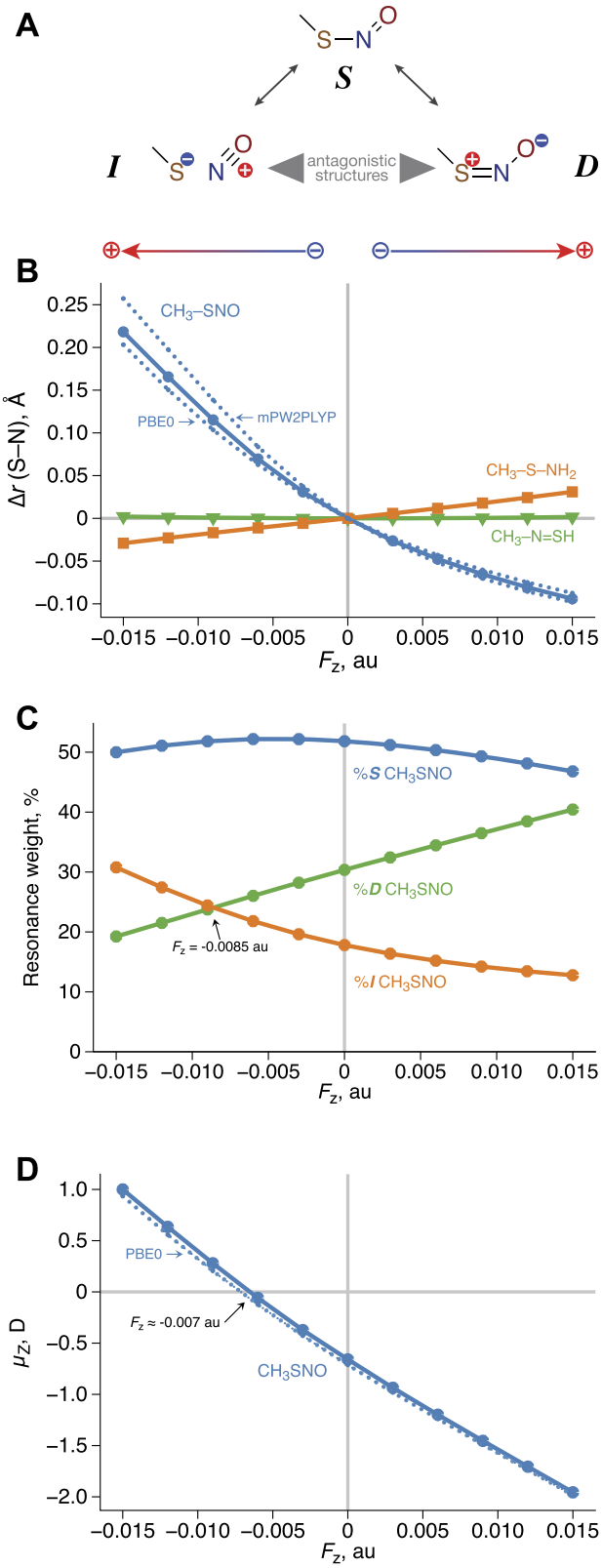

FIG. 3. Resonance description of the electronic structure of the —SNO group as a combination of conventional resonance structure ***S*** (single S—N bond), and antagonistic resonance structures ***D*** (double S—N bond) and ***I*** (ion pair) (a); EEF effects on the S—N bond lengths in CH_3SNO, CH_3NS, and CH_3SNH_2 molecules, calculated with CCSD(T)-F12/VDZ-F12, PBE0/def2-TZVPPD, and mPW2PLYP/def2-TZVPPD methods (b); EEF effects on the resonance weights obtained from PBE0/def2-TZVPPD calculations of *cis*-CH_3SNO optimized in EEF (c); and dependence of the dipole moment projections μ_Z on the S—N vector calculated with CCSD(T)-F12/VDZ-F12 and PBE0/def2-TZVPPD for relaxed *cis*-CH_3SNO geometries (d).

in *cis*-CH_3SNO and *cis*-HSNO, respectively) and 2.7 kcal/mol stronger (D_0 is 32.4 vs 29.7 in *cis*-CH_3SNO and *trans*-HSNO), and the rotation barrier is ~3 kcal/mol higher ($E_0^{\neq}$ is 12.7 vs. 9.5 kcal/mol).[28] This is consistent with the electron-donating character of the CH_3— group that favors the structure ***D*** with a positive formal charge on the sulfur atom and double S=N bond. The transition structure for the rotation along the S—N bond correlates well with the removal of the resonance structure ***D*** that otherwise counteracts the effect of the ionic no-bond resonance structure ***I***. This leads to dramatic lengthening of the S—N bond to >1.9 Å, well beyond the distance expected for a covalent bond involving these atoms. Importantly, the variation of the S—N bond in *cis*- and *trans*-CH_3SNO and the $TS_{c\text{-}t}$ structure anti-correlates with the N—O bond length, in agreement with the antagonistic resonance description [Fig. 3(a)].

However, a more direct way to probe the antagonistic nature of the —SNO group is to observe the effect of an external electric field (EEF) on its properties. If the opposite formal charges implied by the antagonistic structures are to be given credence, one should expect a significant change in the contribution of these structures with attendant significant changes in the S—N bond length. Indeed, optimization of the CH_3SNO geometry in an EEF oriented along the S—N bond, F_Z, varied from +0.015 to −0.015 a.u. (1 a.u. = 51.4 V/Å), leads to dramatic changes in the S—N bond length, much larger than the corresponding changes observed for typical single and double S—N bonds [Fig. 3(b)]. The effect is particularly well pronounced for the negative F_Z values that lead to >0.2 Å lengthening of the S—N bond due to the increasing contribution of the structure ***I*** and decreasing contribution of the structure ***D***. On the other hand, shortening of the S—N bond in the positive fields is smaller, up to 0.1 Å. Scanning the EEF oriented along the S—O axis gives essentially the same results (Fig. S2 of the supplementary material).

DFT methods reproduce the S—N bond variation $\triangle r$(S—N) in EEF, with PBE0 only slightly underestimating the shortening of the positive fields, and the double hybrid mPW2PLYP method slightly overestimating $\triangle r$(S—N) across the board [Fig. 3(b)]. The evolution of the —SNO group electronic structure can be conveniently quantified by the analysis of the DFT density matrix with natural resonance theory (NRT), which expresses the density matrix in terms of the resonance contributions of several Lewis structures. NRT calculations [Fig. 3(c)] show that the dominant structure ***S*** has a fairly constant contribution %***S*** within the F_Z range studied, whereas the ***D*** structure contribution changes linearly with the electric field. The variation of the structure ***I*** contribution %***I*** is slightly non-linear, mirroring the nonlinearity in the %***S*** evolution, with a positive (%***I***) and a negative (%***S***) curvature. This nonlinearity correlates with a similar curving of $\triangle r$(S—N) vs. F_Z dependence and can be attributed to the slower decrease of %***I*** in $F_Z > 0$, so the linear increase in %***D*** has to be compensated by additional %***S*** decrease.

At $F_Z = 0$, structure ***D*** has a higher contribution than ***I***; as F_Z increases in the negative direction, %***I*** increases at the expense of %***D***. At $F_Z \approx -0.0085$ a.u., the ***D*** and ***I*** contributions balance out, and ***I*** becomes the dominant antagonistic structure beyond that point. Remarkably, this changeover

in *%**D*** and *%**I*** nearly coincides with the molecular dipole moment projection [Fig. 3(d)] onto the S—N axis μ_Z reaching zero at −0.007 a.u. [−0.0065 a.u. for CCSD(T)–F12]. For the fields above this critical value, the orientation of the dipole moment is consistent with positively charged sulfur atom and negatively charged NO moiety, i.e., the predominance of the structure ***D***; in the more negative fields, the dipole moment is reversed, consistent with the predominance of the structure ***I***.

We also used EEF to probe the transition structure for rotation along the S—N bond $TS_{c\text{-}t}$ [Fig. 4(a)]. Although the S—N bond in the $TS_{c\text{-}t}$ is significantly longer, the evolution of its relative change $\triangle r$(S—N) is very similar to that of *cis*-CH_3SNO, with the main difference that the S—N lengthening in the TS is slower for $F_Z < -0.005$ a.u. [Fig. 4(b)]. Although the contribution of structure ***D*** is nearly negligible [but not zero due to a slightly non-perpendicular dihedral angle, ∼85°, Fig. 4(c)], *%**I*** is only slightly larger (by ≈3%) than in *cis*-CH_3SNO; however, in the absence of structure ***D***, it is sufficient to significantly weaken the S—N bond. The evolution of the dipole moment projection μ_Z is similar to *cis*-CH_3SNO, but shifted by approximately 0.007 a.u. toward the positive values, reflecting the stronger effect of the structure ***I*** [Fig. 4(d)].

The EEF effect on the S—N bond in *cis*-CH_3SNO is determined by an interplay between the agonistic structures ***D*** and ***I***, but for $TS_{c\text{-}t}$, the EEF effect is mainly due an interplay between the one remaining antagonistic structure ***I*** and the dominant conventional structure ***S*** [Figs. 3(a) and 4(a), correspondingly]. Although this underlying difference is not immediately evident from the evolution of the S—N bond length, it can be gleaned from the evolution of the N—O bond length (Fig. 5). Indeed, r(N—O) vs. F_Z has a larger slope for *cis*-CH_3SNO because ***D*** and ***I*** interconversion causes more significant change in the N—O bond nature (single vs. triple). The slope is smaller in the case of the $TS_{c\text{-}t}$ structure since the N—O bond nature change is less dramatic for ***I*** and ***S*** interconversion (triple vs. double).

Thus, analysis of the physical observables (geometry and dipole moment) obtained with *ab initio* and DFT calculations supports the antagonistic model of the —SNO group, a powerful conceptual model that can be conveniently quantified using the NRT analysis. This study also shows that DFT methods are capable of correctly capturing the evolution of the —SNO group properties across a wide range of

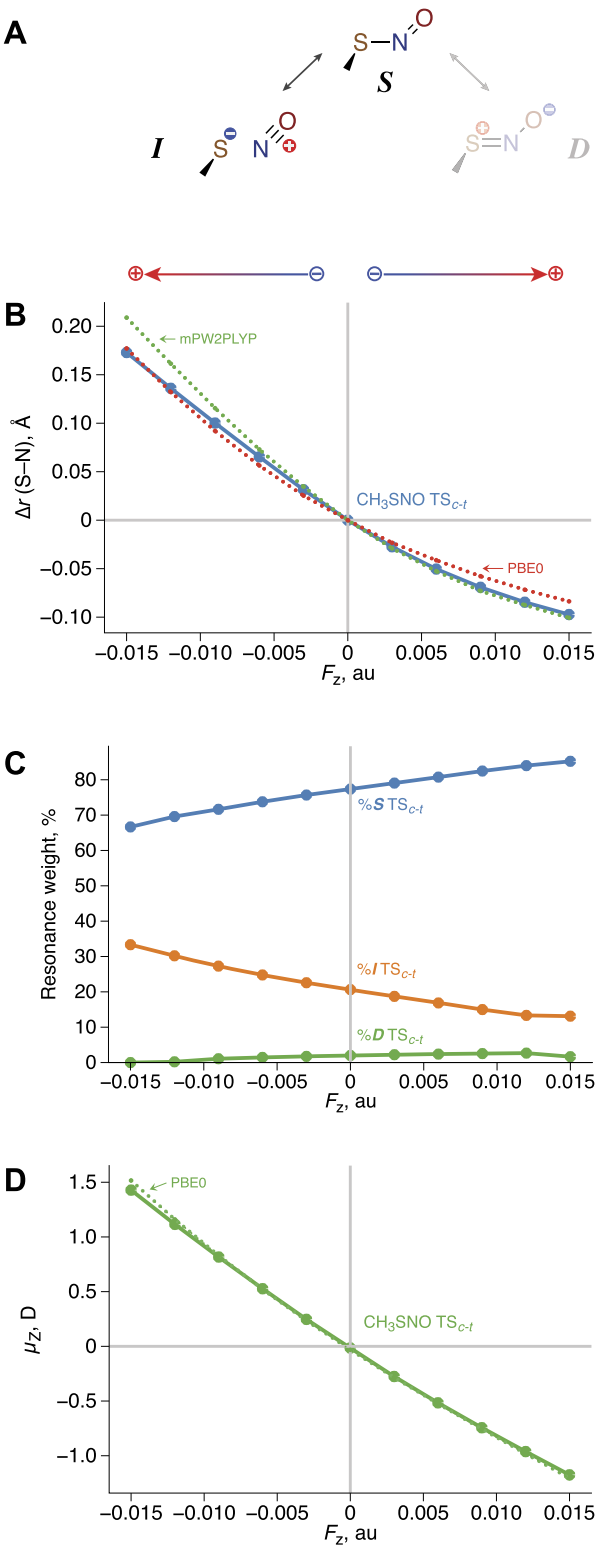

FIG. 4. Resonance description of the electronic structure of the —SNO group in $TS_{c\text{-}t}$ (a); EEF effects on the S—N bond lengths in $TS_{c\text{-}t}$, calculated with CCSD(T)-F12/VDZ-F12, PBE0/def2-TZVPPD, and mPW2PLYP/def2-TZVPPD methods (b); EEF effects on the resonance weights obtained from PBE0/def2-TZVPPD calculations (c); and dependence of the dipole moment projections μ_Z on the S—N vector calculated with CCSD(T)-F12/VDZ-F12 and PBE0/def2-TZVPPD for $TS_{c\text{-}t}$ geometries (d).

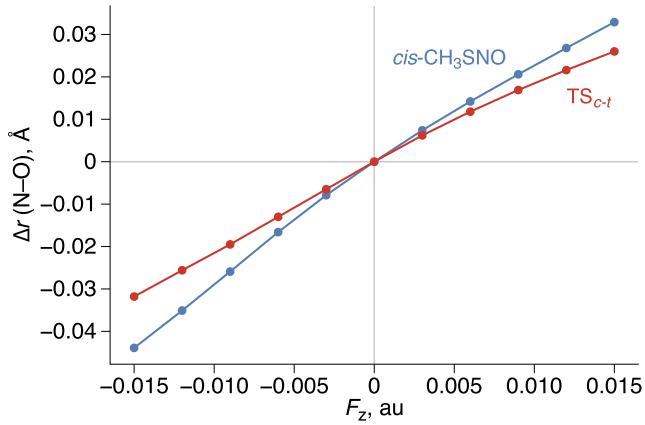

FIG. 5. EEF effect on the N—O bond lengths in *cis*-CH_3SNO and $TS_{c\text{-}t}$, calculated with CCSD(T)-F12/VDZ-F12 methods.

external perturbations. Finally, it has been hypothesized that biochemical reactions can be controlled by electric fields created in proteins, which can reach up to ±0.01 a.u.[102–108] This suggests a possible mechanism of effective biological control of protein CysNO reactivity that takes advantage of the peculiar antagonistic nature of the —SNO group.

IX. CONCLUSIONS

In this work, we reported accurate *ab initio* calculations of the structure and properties of CH_3SNO (summarized in Fig. 2) using the Feller-Peterson-Dixon (FPD) approach based on the explicitly correlated coupled-cluster methodology with extrapolation to the complete basis set limit with several additive corrections. These accurate computational data on CH_3SNO, the smallest aliphatic S-nitrosothiol (RSNO), provide a useful estimation of the intrinsic properties of the S—N bond in S-nitrosated cysteine aminoacid residue (CysNO) sidechain. Compared to a smaller RSNO model molecule—and likely also a biological RSNO itself—thionitrous acid HSNO, the S—N bond in CH_3SNO is ∼0.03 Å shorter, ∼3 kcal/mol stronger, and has ∼3 kcal/mol higher rotational barrier. While the energetic difference between cis- and trans-conformers is roughly the same, ∼1 kcal/mol, CH_3SNO prefers the cis-orientation of the NO moiety, whereas HSNO prefers the trans-form.

While introduction of efficient explicitly correlated coupled-cluster methods alleviates the slow convergence of the S—N bond properties with the one-electron basis set size, slow convergence with the coupled-cluster excitation level remains a problem. Although the recently developed distinguished cluster approximation, DCSD, works significantly better than the traditional CCSD method, it falls short of the coupled-cluster methods that include triple and quadruple excitations. Fortunately, some commonly used density functional theory methods, such as PBE0 and mPW2PLYPD tested in this work, provide a reasonably accurate description of the —SNO group at a modest computational cost.

Curiously, the evolution of the S—N bond properties with respect to the level of correlation treatment is rather counterintuitive. As the coupled-cluster description improves, this bond becomes longer and floppier and, at the same time, harder to dissociate or rotate around. On transition from CCSD to CCSDT(Q), the calculated S—N bond in CH_3SNO becomes >0.05 Å longer (1.794 Å to 1.817 Å, estimated CBS limit, see also Table S2 of the supplementary material) and its stretching force constant drops by >0.2 mdyn/Å (0.8 to 0.56 mdyn/Å, estimated with a double-zeta basis set, Table S22 of the supplementary material), while its bond dissociation energy increases by >7.7 kcal/mol (D_e = 27.7 to 35.4 kcal/mol, estimated CBS limit) and the rotation barrier increases by ∼1.4 kcal/mol (11.8 to 13.2 kcal/mol, estimated CBS limit). All this points out to a rather unusual and complex, multi-reference character of the —SNO group.

Conceptually, the properties of CH_3SNO (as well as other RSNO molecules) can be understood through the antagonistic resonance model that represents its chemical structure as a hybrid of three Lewis structures [Fig. 3(a)], two of which are chemical opposites of each other—antagonistic structures. This model can be quantified using the natural resonance theory (NRT) approach and tested by monitoring the —SNO group response to the external electric fields (EEFs). Remarkably, the inversion of the dipole moment projection observed for CH_3SNO in moderately strong EEF appears to correlate with inversion of the relative order of the resonance contributions of the two antagonistic structures calculated with NRT.

It is interesting to consider if there is a relation between the antagonistic nature and the multireference character of the —SNO group. As we have seen in this work, the calculated S—N bond length in the cis-trans interconversion transition structure $TS_{c\text{-}t}$ converges with the coupled-cluster excitation level at least as slowly as in the equilibrium structures (e.g., Table S22 of the supplementary material). As the S—N bond in $TS_{c\text{-}t}$ loses its double-bond character, this seems to support our hypothesis[81] that connects the ionic component RS^-/NO^+ and the multi-reference character of the —SNO group. Since the unusual electronic structure of the —SNO group likely plays a defining role in the biological reactivity of RSNOs, further investigations in this direction are warranted.

SUPPLEMENTARY MATERIAL

See supplementary material for the *ab initio* and DFT structural, spectroscopic, and energetic parameters of the CH_3SNO isomers (Tables S1-S22, Figs. S1-S2).

ACKNOWLEDGMENTS

This work has been supported by the National Science Foundation (NSF) CAREER Award No. CHE-1255641 and the Extreme Science and Engineering Discovery Environment (XSEDE) allocation under "Computational Modeling of Biologically Important S-Nitrosothiol Reactions" Project No. TG-CHE140079 (Q.K.T.). Calculations were performed on the high-performance dedicated XSEDE cluster *Comet* and on the computational cluster *Père* at Marquette University funded by NSF Award Nos. OCI-0923037 and CBET-0521602.

[1] K. A. Broniowska, A. R. Diers, and N. Hogg, Biochim. Biophys. Acta **1830**, 3173 (2013).
[2] K. A. Broniowska and N. Hogg, Antioxid. Redox Signaling **17**, 969 (2012).
[3] J. R. Lancaster, Arch. Biochem. Biophys. **617**, 137 (2016).
[4] B. C. Smith and M. A. Marletta, Curr. Opin. Chem. Biol. **16**, 498 (2012).
[5] T. Nakamura and S. A. Lipton, Trends Pharmacol. Sci. **37**, 73 (2016).
[6] D. T. Hess, A. Matsumoto, S.-O. Kim, H. E. Marshall, and J. S. Stamler, Nat. Rev. Mol. Cell Biol. **6**, 150 (2005).
[7] S. M. Haldar and J. S. Stamler, J. Clin. Invest. **123**, 101 (2013).
[8] D. Seth and J. S. Stamler, Curr. Opin. Chem. Biol. **15**, 129 (2011).
[9] T. Nakamura and S. A. Lipton, Antioxid. Redox Signaling **18**, 239 (2013).
[10] N. Gould, P.-T. Doulias, M. Tenopoulou, K. Raju, and H. Ischiropoulos, J. Biol. Chem. **288**, 26473 (2013).
[11] A. Feechan, E. Kwon, B.-W. Yun, Y. Wang, J. A. Pallas, and G. J. Loake, Proc. Natl. Acad. Sci. U. S. A. **102**, 8054 (2005).
[12] M. Zaffagnini, M. De Mia, S. Morisse, N. Di Giacinto, C. H. Marchand, A. Maes, S. D. Lemaire, and P. Trost, Biochim. Biophys. Acta **1864**, 952 (2016).
[13] D. Seth, A. Hausladen, Y.-J. Wang, and J. S. Stamler, Science **336**, 470 (2012).
[14] P. Anand and J. S. Stamler, J. Mol. Med. **90**, 233 (2012).
[15] J. S. Stamler and D. T. Hess, Nat. Cell Biol. **12**, 1024 (2010).

[16]D. L. H. Williams, J. Chem. Soc., Chem. Commun. 1758 (1993).
[17]D. L. H. Williams, Acc. Chem. Res. **32**, 869 (1999).
[18]M. D. Bartberger, J. D. Mannion, S. C. Powell, J. S. Stamler, K. N. Houk, and E. J. Toone, J. Am. Chem. Soc. **123**, 8868 (2001).
[19]C. C. Gaucher, A. Boudier, F. Dahboul, M. Parent, and P. Leroy, Curr. Pharm. Des. **19**, 458 (2013).
[20]M. R. Talipov and Q. K. Timerghazin, J. Phys. Chem. B **117**, 1827 (2013).
[21]Q. K. Timerghazin and M. R. Talipov, J. Phys. Chem. Lett. **4**, 1034 (2013).
[22]W. H. Koppenol, Inorg. Chem. **51**, 5637 (2012).
[23]Y. Fu, Y. Mou, B.-L. Lin, L. Liu, and Q.-X. Guo, J. Phys. Chem. A **106**, 12386 (2002).
[24]C. Baciu and J. W. Gauld, J. Phys. Chem. A **107**, 9946 (2003).
[25]Q. K. Timerghazin, G. H. Peslherbe, and A. M. English, Phys. Chem. Chem. Phys. **10**, 1532 (2008).
[26]B. Nagy, P. Szakács, J. Csontos, Z. Rolik, G. Tasi, and M. Kállay, J. Phys. Chem. A **115**, 7823 (2011).
[27]M. Hochlaf, R. Linguerri, and J. S. Francisco, J. Chem. Phys. **139**, 234304 (2013).
[28]L. V. Ivanova, B. J. Anton, and Q. K. Timerghazin, Phys. Chem. Chem. Phys. **16**, 8476 (2014).
[29]M. Méndez, J. S. Francisco, and D. A. Dixon, Chem. - Eur. J. **20**, 10231 (2014).
[30]M. Nava, M.-A. Martin-Drumel, C. A. Lopez, K. N. Crabtree, C. C. Womack, T. L. Nguyen, S. Thorwirth, C. C. Cummins, J. F. Stanton, and M. C. McCarthy, J. Am. Chem. Soc. **138**, 11441 (2016).
[31]J. L. Miljkovic, I. Kenkel, I. Ivanović-Burmazović, and M. R. Filipovic, Angew. Chem., Int. Ed. **52**, 12061 (2013).
[32]M. R. Filipovic, J. L. Miljkovic, T. Nauser, M. Royzen, K. Klos, T. Shubina, W. H. Koppenol, S. J. Lippard, and I. Ivanović-Burmazović, J. Am. Chem. Soc. **134**, 12016 (2012).
[33]B. S. King, Free Rad. Biol. Med. **55**, 1 (2012).
[34]M. Flister and Q. K. Timerghazin, J. Phys. Chem. A **118**, 9914 (2014).
[35]T. B. Adler, G. Knizia, and H.-J. Werner, J. Chem. Phys. **127**, 221106 (2007).
[36]G. Knizia, T. B. Adler, and H.-J. Werner, J. Chem. Phys. **130**, 054104 (2009).
[37]G. Rauhut, G. Knizia, and H.-J. Werner, J. Chem. Phys. **130**, 054105 (2009).
[38]D. Khomyakov, M.S. thesis, Marquette University, 2015.
[39]D. Feller, K. A. Peterson, and D. A. Dixon, Mol. Phys. **110**, 2381 (2012).
[40]K. A. Peterson, D. Feller, and D. A. Dixon, Theor. Chem. Acc. **131**, 1079 (2012).
[41]D. A. Dixon, D. Feller, K. A. Peterson, R. A. Wheeler, and G. S. Tschumper, Annu. Rep. Comput. Chem. **8**, 1 (2012).
[42]H.-J. Werner, P. J. Knowles, G. Knizia, F. R. Manby, and M. Schütz, Wiley Interdiscip. Rev.: Comput. Mol. Sci. **2**, 242 (2012).
[43]J. F. Stanton, J. Gauss, M. E. Harding, P. G. Szalay, A. A. Auer, R. J. Bartlett, U. Benedikt, C. Berger, D. E. Bernholdt, and Y. J. Bomble, CFOUR 1.0, 2009, http://www.cfour.de.
[44]M. Kállay, MRCC, a String-based Quantum Chemical Program Suite, http://www.mrcc.hu.
[45]K. A. Peterson, T. B. Adler, and H.-J. Werner, J. Chem. Phys. **128**, 084102 (2008).
[46]D. Kats and F. R. Manby, J. Chem. Phys. **139**, 021102 (2013).
[47]D. Kats, J. Chem. Phys. **141**, 061101 (2014).
[48]D. Kats, D. Kreplin, H.-J. Werner, and F. R. Manby, J. Chem. Phys. **142**, 064111 (2015).
[49]K. A. Peterson, D. E. Woon, and T. H. Dunning, Jr., J. Chem. Phys. **100**, 7410 (1994).
[50]J. G. Hill, S. Mazumder, and K. A. Peterson, J. Chem. Phys. **132**, 054108 (2010).
[51]M. Douglas and N. M. Kroll, Ann. Phys. **82**, 89 (1974).
[52]G. Jansen and B. A. Hess, Phys. Rev. A **39**, 6016 (1989).
[53]D. W. Schwenke, J. Chem. Phys. **122**, 014107 (2005).
[54]J. G. Hill, K. A. Peterson, G. Knizia, and H.-J. Werner, J. Chem. Phys. **131**, 194105 (2009).
[55]D. G. Fedorov, S. Koseki, M. W. Schmidt, and M. S. Gordon, Int. Rev. Phys. Chem. **22**, 551 (2003).
[56]H.-J. Werner and P. J. Knowles, J. Chem. Phys. **89**, 5803 (1988).
[57]P. J. Knowles and H.-J. Werner, Chem. Phys. Lett. **145**, 514 (1988).
[58]T. H. Dunning, Jr., J. Chem. Phys. **90**, 1007 (1989).
[59]T. H. Dunning, Jr., K. A. Peterson, and A. K. Wilson, J. Chem. Phys. **114**, 9244 (2001).
[60]M. J. Frisch, G. W. Trucks, H. B. Schlegel, G. E. Scuseria, M. A. Robb, J. R. Cheeseman, G. Scalmani, V. Barone, B. Mennucci, G. A. Petersson, H. Nakatsuji, M. Caricato, X. Li, H. P. Hratchian, A. F. Izmaylov, J. Bloino, G. Zheng, J. L. Sonnenberg, M. Hada, M. Ehara, K. Toyota, R. Fukuda, J. Hasegawa, M. Ishida, T. Nakajima, Y. Honda, O. Kitao, H. Nakai, T. Vreven, J. A. Montgomery, Jr., J. E. Peralta, F. Ogliaro, M. Bearpark, J. J. Heyd, E. Brothers, K. N. Kudin, V. N. Staroverov, R. Kobayashi, J. Normand, K. Raghavachari, A. Rendell, J. C. Burant, S. S. Iyengar, J. Tomasi, M. Cossi, N. Rega, J. M. Millam, M. Klene, J. E. Knox, J. B. Cross, V. Bakken, C. Adamo, J. Jaramillo, R. Gomperts, R. E. Stratmann, O. Yazyev, A. J. Austin, R. Cammi, C. Pomelli, J. W. Ochterski, R. L. Martin, K. Morokuma, V. G. Zakrzewski, G. A. Voth, P. Salvador, J. J. Dannenberg, S. Dapprich, A. D. Daniels, Ö. Farkas, J. B. Foresman, J. V. Ortiz, J. Cioslowski, and D. J. Fox, GAUSSIAN 09, Revision D.01, Gaussian, Inc., Wallingford, CT, 2009.
[61]A. D. Becke, Phys. Rev. A **38**, 3098 (1988).
[62]C. Lee, W. Yang, and R. G. Parr, Phys. Rev. B **37**, 785 (1988).
[63]P. J. Stephens, F. J. Devlin, C. F. Chabalowski, and M. J. Frisch, J. Phys. Chem. **98**, 11623 (1994).
[64]C. Adamo and V. Barone, J. Chem. Phys. **110**, 6158 (1999).
[65]J. P. Perdew, K. Burke, and M. Ernzerhof, Phys. Rev. Lett. **77**, 3865 (1996).
[66]M. Ernzerhof and G. E. Scuseria, J. Chem. Phys. **110**, 5029 (1999).
[67]S. Grimme, J. Antony, S. Ehrlich, and H. Krieg, J. Chem. Phys. **132**, 154104 (2010).
[68]C. A. Guido, E. Brémond, C. Adamo, and P. Cortona, J. Chem. Phys. **138**, 021104 (2013).
[69]J.-D. Chai and M. Head-Gordon, Phys. Chem. Chem. Phys. **10**, 6615 (2008).
[70]E. Brémond and C. Adamo, J. Chem. Phys. **135**, 024106 (2011).
[71]E. Brémond, J. C. Sancho-García, Á. José Pérez-Jiméne, and C. Adamo, J. Chem. Phys. **141**, 031101 (2014).
[72]S. Grimme, J. Chem. Phys. **124**, 034108 (2006).
[73]T. Schwabe and S. Grimme, Phys. Chem. Chem. Phys. **8**, 4398 (2006).
[74]F. Weigend and R. Ahlrichs, Phys. Chem. Chem. Phys. **7**, 3297 (2005).
[75]D. Rappoport and F. Furche, J. Chem. Phys. **133**, 134105 (2010).
[76]E. D. Glendening and F. Weinhold, J. Comput. Chem. **19**, 593 (1998).
[77]F. Weinhold and C. R. Landis, *Valency and Bonding: A Natural Bond Orbital Donor-Acceptor Perspective* (Cambridge University Press, 2005).
[78]E. D. Glendening, J. K. Badenhoop, A. E. Reed, J. E. Carpenter, J. A. Bohmann, C. M. Morales, and F. Weinhold, NBO 5.9, Theoretical Chemistry Institute, University of Wisconsin, Madison, 2004.
[79]V. Barone, J. Chem. Phys. **122**, 014108 (2005).
[80]J. Tomasi, B. Mennucci, and R. Cammi, Chem. Rev. **105**, 2999 (2005).
[81]Q. K. Timerghazin, A. M. English, and G. H. Peslherbe, Chem. Phys. Lett. **454**, 24 (2008).
[82]T. J. Lee and P. R. Taylor, Int. J. Quantum Chem. **36**, 199 (1989).
[83]C. L. Janssen and I. M. Nielsen, Chem. Phys. Lett. **290**, 423 (1998).
[84]B. Roy, A. D. M. d'Hardemare, and M. Fontecave, J. Org. Chem. **59**, 7019 (1994).
[85]J. E. Sansonetti and W. C. Martin, J. Phys. Chem. Ref. Data **34**, 1559 (2005).
[86]T. Hrenar, H.-J. Werner, and G. Rauhut, J. Chem. Phys. **126**, 134108 (2007).
[87]M. Neff and G. Rauhut, J. Chem. Phys. **131**, 124129 (2009).
[88]L. Field, R. V. Dilts, R. Ravichandran, P. G. Lenhert, and G. E. Carnahan, J. Chem. Soc., Chem. Commun. 249 (1978).
[89]G. E. Carnahan, P. G. Lenhert, and R. Ravichandran, Acta Crystallogr., Sect. B: Struct. Crystallogr. Cryst. Chem. **34**, 2645 (1978).
[90]N. Arulsamy, D. S. Bohle, J. A. Butt, G. J. Irvine, P. A. Jordan, and E. Sagan, J. Am. Chem. Soc. **121**, 7115 (1999).
[91]R. J. Philippe, J. Mol. Spectrosc. **6**, 492 (1961).
[92]D. H. Christensen, N. Rastrup-Andersen, D. Jones, P. Klabof, and E. R. Lippincott, Spectrochim. Acta, Part A **24**, 1581 (1968).
[93]R. P. Müller and J. R. Huber, J. Phys. Chem. **88**, 1605 (1984).
[94]A. Cánneva, C. O. Della Védova, N. W. Mitzel, and M. F. Erben, J. Phys. Chem. A **119**, 1524 (2014).
[95]A. Canneva, M. F. Erben, R. M. Romano, Yu. V. Vishnevskiy, C. G. Reuter, N. W. Mitzel, and C. O. Della Védova, Chem. - Eur. J. **21**, 10436 (2015).
[96]T. Schwabe and S. Grimme, Phys. Chem. Chem. Phys. **9**, 3397 (2007).
[97]L. V. Ivanova, D. Cibich, G. Deye, M. R. Talipov, and Q. K. Timerghazin, ChemBioChem **18**, 726 (2017).
[98]Q. K. Timerghazin, G. H. Peslherbe, and A. M. English, Org. Lett. **9**, 3049 (2007).
[99]M. R. Talipov, D. G. Khomyakov, M. Xian, and Q. K. Timerghazin, J. Comput. Chem. **34**, 1527 (2013).
[100]B. Meyer, A. Genoni, A. Boudier, P. Leroy, and M. Ruiz-Lopez, J. Phys. Chem. A **120**, 4191 (2016).

[101]E. E. Moran, Q. K. Timerghazin, E. Kwong, and A. M. English, J. Phys. Chem. B **115**, 3112 (2011).
[102]R. Meir, H. Chen, W. Lai, and S. Shaik, Chem. Phys. Phys. Chem. **11**, 301 (2010).
[103]P. M. de Biase, F. Doctorovich, D. H. Murgida, and D. A. Estrin, Chem. Phys. Lett. **434**, 121 (2007).
[104]P. M. de Biase, D. A. Paggi, F. Doctorovich, P. Hildebrandt, D. A. Estrin, D. H. Murgida, and M. A. Marti, J. Am. Chem. Soc. **131**, 16248 (2009).
[105]H. Hirao, H. Chen, M. A. Carvajal, Y. Wang, and S. Shaik, J. Am. Chem. Soc. **130**, 3319 (2008).
[106]W. Lai, H. Chen, K.-B. Cho, and S. Shaik, J. Phys. Chem. Lett. **1**, 2082 (2010).
[107]S. Shaik, S. P. de Visser, and D. Kumar, J. Am. Chem. Soc. **126**, 11746 (2004).
[108]P. J. Aittala, O. Cramariuc, and T. I. Hukka, J. Chem. Theory Comput. **6**, 805 (2010).